Numerical Modeling of Hygrothermal Response in a Full-Scale Experimental Room and through the Envelope

Yang Li **Paul Fazio, PhD** **Jiwu Rao, PhD**

ABSTRACT

In this paper, the influence of the ventilation rate, vent size, and position of the inlet and outlet on indoor air conditions and on the heat and moisture transport through the envelope are investigated by an experiment-based numerical model. The testing is the extension of an experimental project carried out within International Energy Agency (IEA) Annex 41. The numerical model simulates one test scenario and compares its simulated profile of the indoor temperature and relative humidity with experimental measurements. Close agreement has been obtained. Simulation results show that the position of the ventilation vents has the most significant effect on the indoor environment. The increased ventilation rate carries away more heat and moisture, thus reducing both temperature and moisture levels inside the room. Vent size has the least effect on the indoor environment. Under the mixed convection condition, the indoor temperature and moisture levels, which depend on the ventilation conditions, dominate the heat and moisture transport through the wall system. This investigation is achieved in a single simulation environment: COMSOL, where the CFD and mass transport in the wall is coupled directly. This paper presents the coupling of the momentum, heat, and moisture in the whole simulation domain, including the test room and wall system, with some assumptions.

INTRODUCTION

Moisture level in buildings is a key factor influencing the durability of construction, indoor environmental quality, living comfort, and energy consumption. This level is the result of the dynamic balance of moisture gain, moisture loss, and moisture storage (ASHRAE 2005). This balance depends on the moisture generated from occupants and their activities, the moisture input or removal from HVAC, interzonal moisture flow, air leakage through the building envelope, moisture sink on cold surfaces, and moisture exchange between indoor air and the envelope.

Advanced 3D airflow models have been used to predict the indoor relative humidity and temperature conditions. Such models, however, are not widely applied in simulations that couple vapor diffusion and transport in the indoor air, on one hand, and mass transfer that occurs at the interface of the air and the interior building surfaces, on the other. This is mainly attributed to two facts: the excessive computational time required for such simulations, and the problems related to the validation of these simulations (Paepe 2008).

The Annex 41 research project (2004–2008), under the auspices of the International Energy Agency (IEA), was carried out to explore the complex physics governing whole-building heat, air, and moisture (HAM) transfer. Several models were developed throughout this initiative to couple 3D CFD simulations with hygrothermal models of walls. Due to the limitation of current CFD software that the mass transfer cannot be extended from a fluid region to a solid region, mass coupling between the indoor environment and the wall system was achieved by third-party programming. Basically, the moisture flux on the surface of the wall calculated by CFD was used as the input for the wall model to determine the distribution of the moisture inside the wall material at each time step, and the mass fraction on the wall surface was calculated and sent back to the CFD model as the boundary condition for the next time step. For instance, Neale (2007) solved the heat and

Yang Li *is a PhD candidate,* ***Paul Fazio*** *is a professor, and* ***Jiwu Rao*** *is a research associate in the Department of Building, Civil and Environmental Engineering, Concordia University, Montreal, QC.*

moisture transport in air and porous material by developing a simplified hygrothermal model in MATLAB that was coupled to FLUENT software. By using this model, the moisture surface coefficient is calculated and compared with the Chilton and Colburn analogy results. But the finite-difference model is difficult to extend or modify to fit new simulation conditions. Steeman el al. (2009) used the effective penetration depth (EPD) approach to couple CFD and moisture transport inside the wall. This model has advantages over the well-mixed zonal models in which only the average indoor climate and the average performance of the walls can be predicted. In using this EPD model, the profile of indoor temperature and relative humidity can be obtained in the whole-building simulation, and the local moisture behavior of the wall can be evaluated. While the EPD models do allow the simplified quantification, it has been argued that their reliance on the moisture penetration depth concept necessitates comprehensive material properties (Janssen and Roels 2009). In the EPD model, the penetration depth, which is an estimation value based on the calculation of the sudden moisture level change on the surface of the material, has to be known in the model. This may limit the application and accuracy of the model.

Besides the Annex 41 project, other recent studies were carried out to couple CFD simulations with hygrothermal models of walls. Amissah (2005) coupled a 1D HAM model to a low-Reynolds number k–ε turbulence model, with independent execution and information exchanged at every time step. The HAM model supplied realistic boundary conditions for the CFD simulation, while CFD results supported direct modeling of convective mass transfer. Erriguible et al. (2006) indirectly coupled a 2D CFD model with a 2D hygrothermal material model. In these models, similar limitations can be found, and the main reason is that all these models are not simulated in one single simulation environment. Van Schijndel (2008) outlined the possibility of integrating indoor air CFD and envelope HAM within the COMSOL environment; however, only a guideline to build such models was provided.

This paper presents a coupling model of CFD and heat/moisture transport inside the wall implemented in a single simulation environment (COMSOL). A CFD model is developed, which couples the momentum, heat, and mass transport inside the room and the heat and mass transport inside the wall material. Data from the full-scale experimental program are used to develop the numerical model and as a reference to compare the results of the simulation results. This model is then used to investigate the effect of some building and operation parameters, such as the ventilation inlet and outlet design, on the indoor environment.

APPROACH

Experimental Setup and Test Conditions

The test setup employed in this research is based on an existing setup established for the project within Annex 41 (Fazio et al. 2007; Yang et al. 2007; Vera et al. 2010). The original experiments were conducted to provide data sets of HAM performance and indoor environment response of typical wood-frame Canadian constructions. These tests were carried out using the environmental chamber at Concordia University (Fazio et al. 2007).

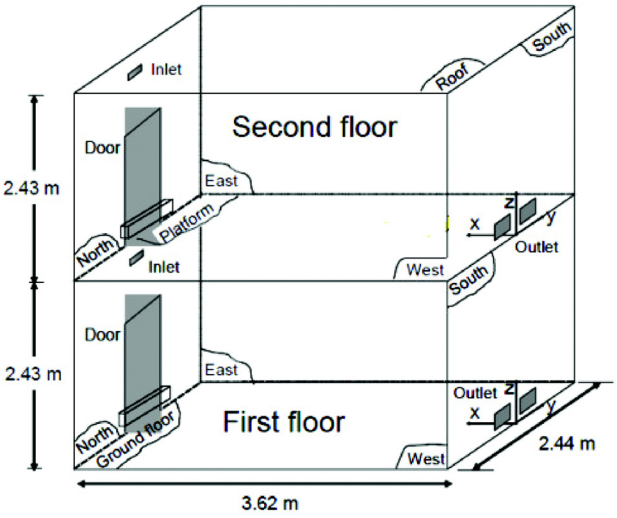

Figure 1 *Schematic drawing of the experimental test hut (adapted from Fazio et al. 2007).*

A two-story test hut (Figure 1) was installed inside the environmental chamber. The room interior on each floor of the test hut had the dimensions of 3.62 m (L) × 2.44 m (D) × 2.43 m (H). The environmental chamber simulated constant outdoor conditions of –5 °C and 68% RH. While both floors were used in the previous project (Fazio et al. 2007), only the first floor was used for the current experiment.

The walls in each room were built according to the typical wood-frame Canadian construction standards (2 in. × 6 in. studs with 24 in. center-to-center [cc] spacing). Each of these walls was composed of the following components (from interior to exterior): unpainted drywall, vapor barrier, insulation in the stud cavity, sheathing, and PVC cladding over furring. The east and west walls had an additional layer of wood paneling next to the gypsum board; this layer was used to study the moisture-buffering effect of the wood under the given conditions. The rest of the enclosure (floor, ceiling, door, and north and south walls) was covered with metal sheets to prevent any hygric interaction. The components of the wall configuration are shown in Figure 2.

The studied room was ventilated by a special air-handling unit (AHU). The air and moisture mixture inside the test room was treated by the AHU and returned to the test room at a controlled temperature and humidity ratio. The ventilation rate was 0.5 air change per hour (ACH) for the experimental data in this paper. A metal recipient on a hotplate at the center of the room was used to generate steam. The moisture generation was controlled at 42 g/h by a programmed peristaltic

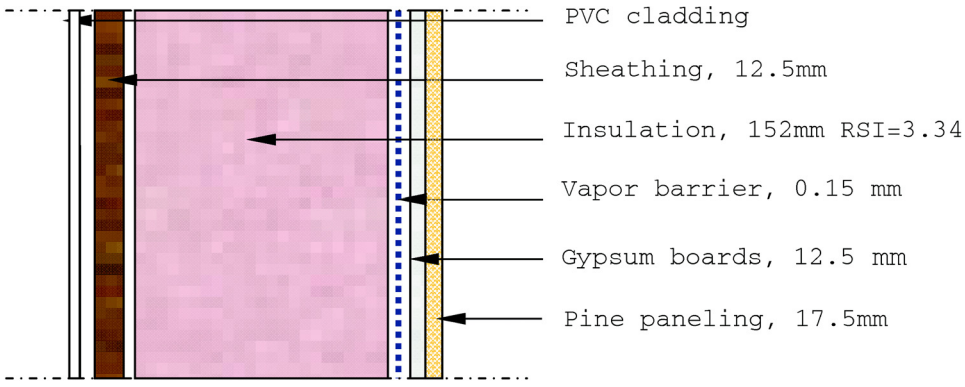

Figure 2 *Configuration of the east and west wall assemblies.*

pump and verified by the load cell. The duration of moisture generation was24 hours. Before moisture generation, the room was preconditioned with supply air of 20°C and 34% RH. Sensors were located in the test room, at the entrances of the inlet and outlet to record the temperature and relative humidity profiles of the indoor environment and of the supply air and exhaust air. Additional details about the experimental setup can be found in Fazio et al. (2007).

Numerical Model

Model Description. The objective of the simulation was to calculate heat and mass transport inside the room and through the wall system. The numerical model was developed in the COMSOL multi-physics environment (COMSOL 2008). Due to the limitation of the computer capacity for CFD simulation, the simulation was run for steady state. The robustness and accuracy of the COMSOL solver was benchmarked by Pepper and Wang (2009)

To take advantage of the symmetry of the test room, only half of the room was simulated in the geometrical model. Three simulation subdomains were specified (Figure 3). Subdomain 1 corresponded to the test room. The wood paneling constituted subdomain 2. Finally, the rest of the wall was represented by subdomain 3. The inner layer of the wall usually plays an important role in the moisture buffering phenomena and thus was represented in the model by a distinct subdomain to enable separate detection of this layer's moisture-buffering characteristics. The buffering effects will be further investigated later. For this paper, constant material properties instead of nonlinear properties of the wood were assigned to both subdomain 2 and 3.

Governing equations. For the airflow in subdomain 1, the ratio of Grashof number to the square of Reynolds number was about 0.75, thus indicating that mixed convection was occurring during the testing. The Gr number was about 1.5×10^{11}, which implies that the airflow is turbulent. Based on these characteristics, the standard k–ε turbulent, weakly compressible Navier-Stokes model, general heat transfer model, and mass convection model were combined in this subdomain. The governing equations to describe the coupled momentum, heat, and mass transfer are presented below in Equations 1, 2, and 3, respectively:

$$\rho(\vec{V}\cdot\nabla)\vec{V} = \nabla\times$$
$$[PI + (\eta+\eta_T)(\nabla\vec{V} + (\nabla\vec{V})^T - (2/3)(\nabla\cdot\vec{V})I) - (2/3)\rho\kappa I] + \vec{F}$$
$$\nabla\cdot(\rho\vec{V}) = 0 \qquad \rho = \rho(P_o, T) \tag{1}$$

where $\vec{V}$ is the velocity (m/s), P is static pressure (Pa), P_0 is the reference pressure (Pa), $\vec{F}$ is body force (N/m^3), I is the unit tensor (dimensionless), ρ is density (kg/m^3) of the moist air, and η_T is the turbulent viscosity (N·s/m^2) calculated by

$$\eta_T = \rho C_\mu k^2/\varepsilon \tag{1a}$$

where C_μ is a model constant (dimensionless), k is turbulent kinetic energy (m^2/s^2), and ε is the dissipation rate of turbulent energy (m^2/s^3), which are determined by

$$\rho\frac{\partial k}{\partial t} - \nabla\cdot[(\eta+\eta_T/\sigma_k)\nabla k] + \rho\vec{V}\cdot\nabla k = \frac{1}{2}\eta_T[\nabla\vec{V} + (\nabla\vec{V})^T]^2 - \rho\varepsilon \tag{1b}$$

$$\rho\frac{\partial \varepsilon}{\partial t} - \nabla\cdot[(\eta+\eta_T/\sigma_\varepsilon)\nabla\varepsilon] + \rho\vec{V}\cdot\nabla\varepsilon = \frac{1}{2}C_{\varepsilon1}\frac{\varepsilon}{k}\eta_T[\nabla\vec{V} + (\nabla\vec{V})^T]^2 - C_{\varepsilon2}\rho\varepsilon/k \tag{1c}$$

where $C_{\varepsilon1}$, $C_{\varepsilon2}$, σ_k, and σ_ε are dimensionless model constants.

$$\nabla\cdot[-(K+K_T)\nabla T] = Q - \rho C_p\vec{V}\cdot\nabla T \tag{2}$$

where T is temperature (K), Q is the heat source (W/m^3), K is thermal conductivity (W/m·K), C_p is the specific heat capacity (J/kg·K) of the moist air, and K_T is the turbulent conductivity (W/m·K), which depends on the turbulent Prandtl number Pr_T and turbulent viscosity,

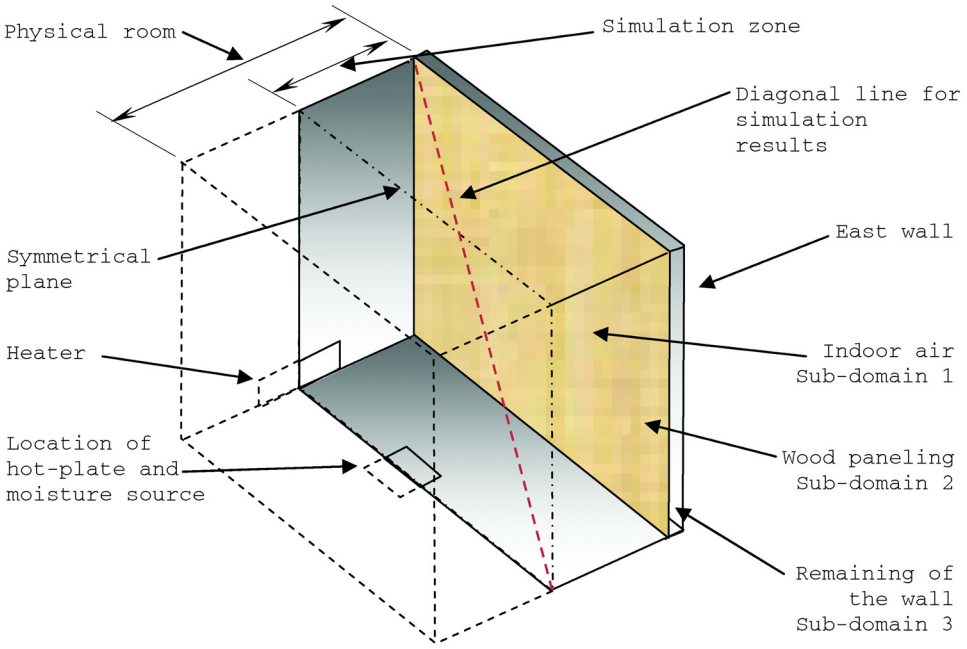

Figure 3 *Schematic of the simulated room, showing the three subdomains and the symmetrical plane.*

$$K_T = C_p \eta_T / \mathrm{Pr}_T \tag{2a}$$

$$\nabla \cdot (-D\nabla c) = R - \vec{V} \cdot \nabla c \tag{3}$$

where D is the diffusion coefficient (kg/m^3·s), c is the moisture concentration (kg/m^3), and R is the reaction rate for mass species (kg/m^3·s).

The coupling procedure among momentum, heat, and mass transport was achieved through Equations 1, 2, and 3. The simultaneous computation of the parameters associated with air velocity, heat, and moisture transport enables in fact to build coupled model. The air density in the momentum transport equation was calculated using the temperature given by the heat transfer equation, while the velocity in heat and mass transport equations and the turbulent kinetic viscosity in heat transfer equations (Equation 2a) were based on the momentum equation (Equation 1).

Heat and mass transfer in subdomain 2 (representing the inner layer of the walls) was governed by the heat conduction equation and mass conservation equation (Equations 2 and 3 with $\vec{V} = 0$).

The continuity of the mass flux is the boundary condition of mass transfer for the interior boundary between subdomains 1 and 2, while the thermal wall function, a heat flux defined in Equation 4, connects the heat transfer equations in the two subdomains:

$$q = \frac{\rho C_p C_\mu^{1/4} k_w^{1/2} (T_w - T)}{T^+} \tag{4}$$

where q is the heat flux (W/m^2), C_μ and k_w are the model constants (dimensionless), T_w is the temperature at wall (K), and dimensionless temperature T^+ is calculated by

$$T^+ = \frac{\mathrm{Pr}_T}{k_r} \ln(\delta_w^+) + \beta$$

where k_r is the von Karman constant (dimensionless), β is a model constant (dimensionless), and δ^+ is a wall offset (dimensionless).

Subdomain 3 included the remaining layers of the wall. The governing equations in subdomain 3 are the same as those used in subdomain 2. To reach the convergence solution and reduce the iterative time, an effective wall was used to simulate the heat and vapor transports in subdomain 3. The effective properties were calculated based on the properties of each wall layer; for example, the effective thermal conductivity was calculated as

$$k_{eff} = \frac{\sum_{i=1}^{n} d_i}{\sum_{i=1}^{n} \frac{d_i}{k_i}} \tag{5}$$

where k_i and d_i are the thermal conductivity and thickness of the ith component.

The unstructured mesh was assigned for the entire calculation domain. The maximum size at inlet surface was set to 0.01 m to 0.02 m at surfaces of outlet, steel recipient, and inner wall surface, and to 0.04 m at heater surface. The global size of the rest of the mesh was set to 0.29 m. The mesh consists of

Table 1. Dimension and Location of Ventilation Vents and Ventilation Rate for Different Cases

	Case 1	Case 2	Case 3	Case 4
Inlet area, m^2	1.05×10^{-3}	1.05×10^{-3}	1.05×10^{-3}	1.05×10^{-3}
Height of the inlet center, m	2.26	2.26	2.26	0.25
Outlet area, m^2	1.15×10^{-2}	1.15×10^{-2}	2.3×10^{-2}	2.3×10^{-2}
Height of the outlet center, m	0.172	0.172	0.172	2.2
Inlet volumetric flow rate, m^3/h	10.73	21.46	10.73	10.73

188,799 elements in subdomain 1 and 46,975 elements in subdomains 2 and 3. In total, 834,546 degrees of freedom were solved in this simulation. The default segregated solvers were selected, with some adjustments. The geometric multigrid solver was used as a preconditioner in the concentration (mass) segregated solver (COMSOL 2008), the damping constant was reduced to 0.3, and variable scaling for mass was defined as 10^{-4} manually.

Implementation of Model

The model described above is implemented in four cases. The first case replicates the same conditions used in the experimental setting. Case 2 is used to investigate the influence of ventilation rate on the indoor environment. The ventilation rate is therefore doubled in this case. The simulation in case 3 uses the normal ventilation rate but a larger outlet area. Case 4 investigates the impact of the position of the inlet and outlet. The dimension and position of the inlet and outlet, together with the flow rate are listed in Table 1. For all cases, the moisture generation rate is 42 g/h. The supply air condition is 20 °C, 45% RH, corresponding to the values used in the experiment. The outdoor conditions are these specified in the experiment (–5 °C, 68% RH) as well.

SIMULATION RESULTS AND DISCUSSION

Figures 4 and 5 show the values of temperature in all subdomains and RH in subdomain 1, respectively. Except for the regions near the heater, hotplate, and inlet, the differences in the temperatures and RH levels inside the room were small (less than 1°C and 3% RH). This is in close agreement with the experimental measurements (Figures 6 and 7). The accuracy is ±0.5°C for temperature measurement and ±2% for RH measurement.

The even temperature and RH distribution inside the test room can be attributed to the air circulation. The maximum measured temperature difference was about 1°C (Figure 6), while the RH difference is 5% (Figure 7). The higher temperatures were recorded by sensor E_11, C_31, and E_31, while the higher RHs are recorded at G_13 and E_35. The same phenomenon was observed in the simulation results, reflecting higher values of temperature and RH at the corresponding locations of the mentioned sensors (Figures 6 and 7).

The overall temperature and moisture concentration profiles obtained from simulation of the indoor air conformed

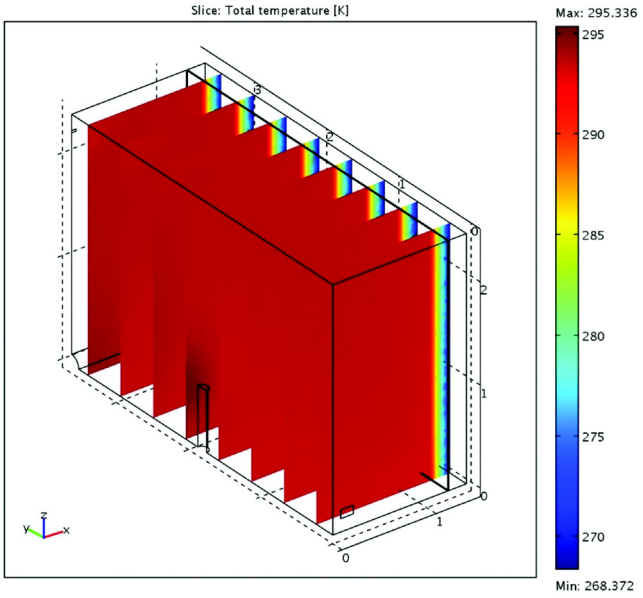

Figure 4 *Simulation result of temperature in the room and across the wall.*

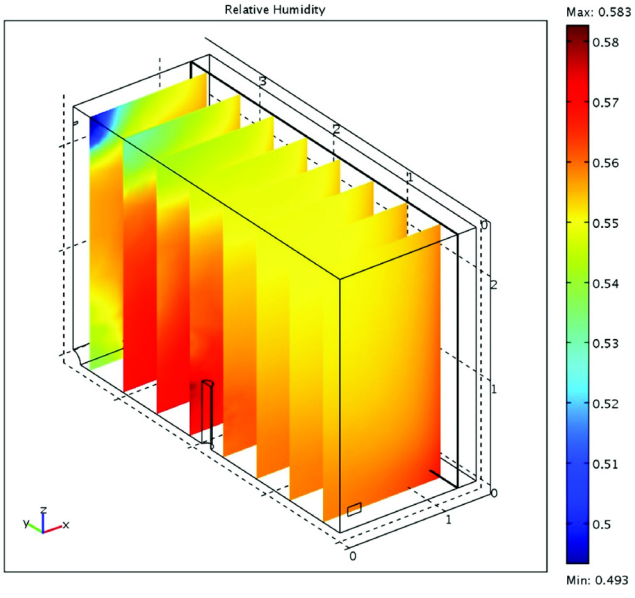

Figure 5 *Simulation result of RH in the room.*

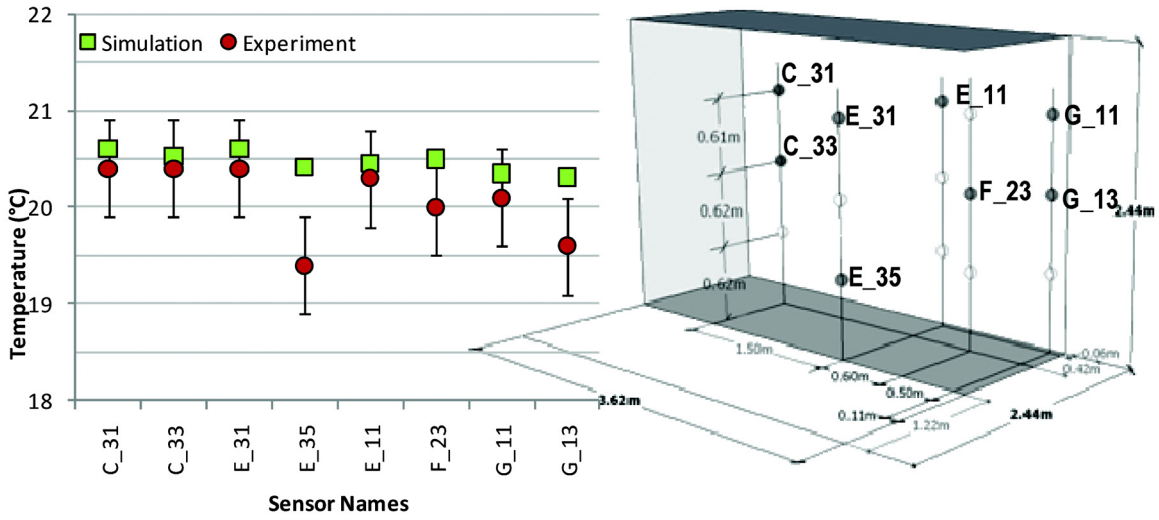

Figure 6 *Comparison of indoor air temperatures between CFD simulation and measurements with ±0.5 ℃ error band in case 1.*

to those recorded by the experiments, as illustrated in Figures 6 and 7. The air temperatures provided by the sensors were slightly lower than those obtained from the simulations. The facts that the test room was not completely airtight and the other interior surfaces except the east and west walls were assumed as the adiabatic in the simulation may be the causes of the temperature differences. The RH results provided by the experiment were higher than those obtained by the simulations, because the computation of RH in the model depended on the temperature results. RH value is, in fact, inversely proportional to the temperature; therefore, a higher temperature implies a lower RH value.

On the other hand, the difference in the amplitude of the results among sensors in the experimental test can be attributed partly to the sensors' accuracies.

Based on this numerical model, the influence of the ventilation rate, size of the ventilation return vent, and position of the inlet and outlet on indoor air conditions and on the heat and moisture transport through the envelope was investigated in cases 2, 3, and 4 respectively.

Figures 8 and 9 show the temperature and RH of subdomain 1, simulated along the diagonal line indicated by the red dashed line in Figure 3. These simulations were performed for all four considered scenarios.

The results indicate that the positions of the inlet and outlet (case 4) have the most significant impact on the indoor environment (Figures 8 and 9). Under the same heat and moisture generation conditions, the average temperature inside the test room in this case was about 2.5°C higher than that obtained in case 1, and the RH value computed in this case was about 18% higher than that of case 1. The large difference is due to the existing heat/mass source at the center of the room. This vent position is not an efficient ventilation design in this scenario. The lower ventilation efficiency keeps more heat and

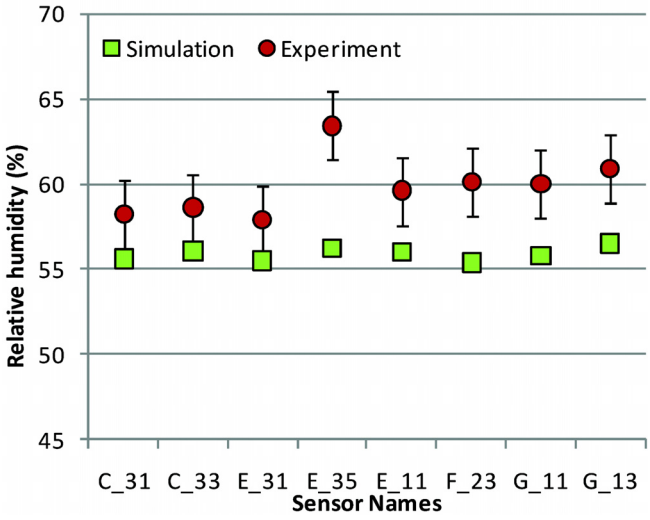

Figure 7 *Comparison of indoor relative humidity levels between CFD simulation and measurements with ±2% error band in case 1.*

moisture generated by the source inside the room and leads to the significant change in the indoor conditions. The movement pattern of the inside air in case 4 (Figure 10) explains why the room with the outlet at a higher position, a beneficial location of exhausting the lighter heated air, still resulted in a higher room temperature. Unlike the other cases where the air was circulated clockwise in the whole test room and then mixed well with the heat and moisture coming from the source, in this scenario, the buoyancy force due to the hotplate separated the air circulation into two parts. One part of the air on the north

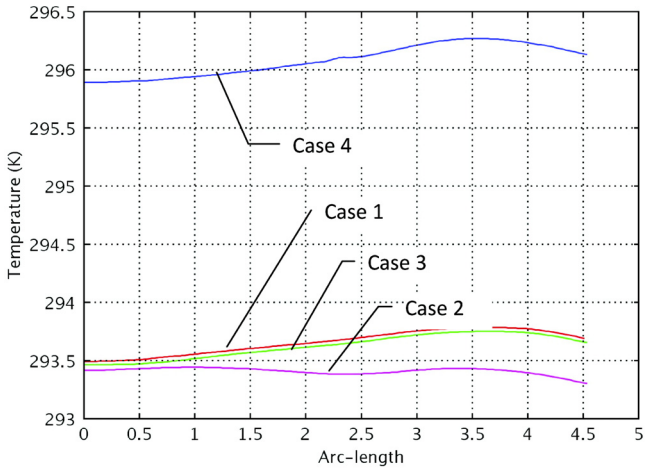

Figure 8 *Temperatures along the straight diagonal line from the bottom center of the south wall to the upper corner of the north and east walls.*

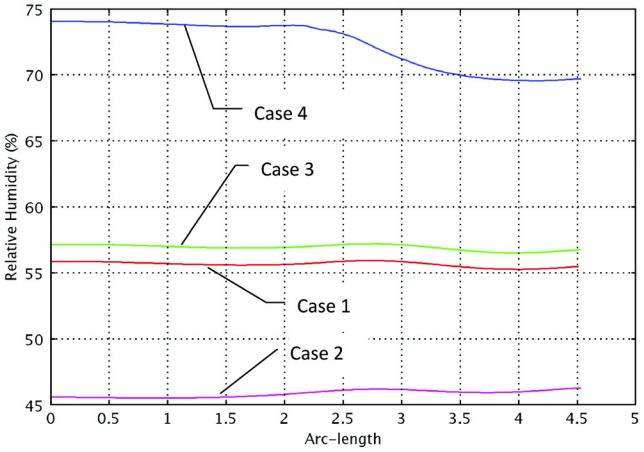

Figure 9 *Relative humidity profiles along the straight line from bottom center of the south wall to the upper corner of the north and east walls.*

side (i.e., the side near the electric heater) circulated counterclockwise due to the jet coming in from the supply vent; the other part of the air on the same side circulated clockwise due to heating by the electric baseboard. This mixed circulation reduced air movement and heats up the air on this side. On the south side, the air circulated clockwise due to the center hotplate. The separated circulations trapped heat and moisture, and made the air inside room not well mixed. This results in a high value of temperature and RH.

The increased ventilation rate (case 2) also has a significant effect on the indoor environment. The average indoor temperature was reduced by 0.5°C with a different distribution profile (Figure 8), and the relative humidity was reduced by 10% under the same heating and moisture generation. The

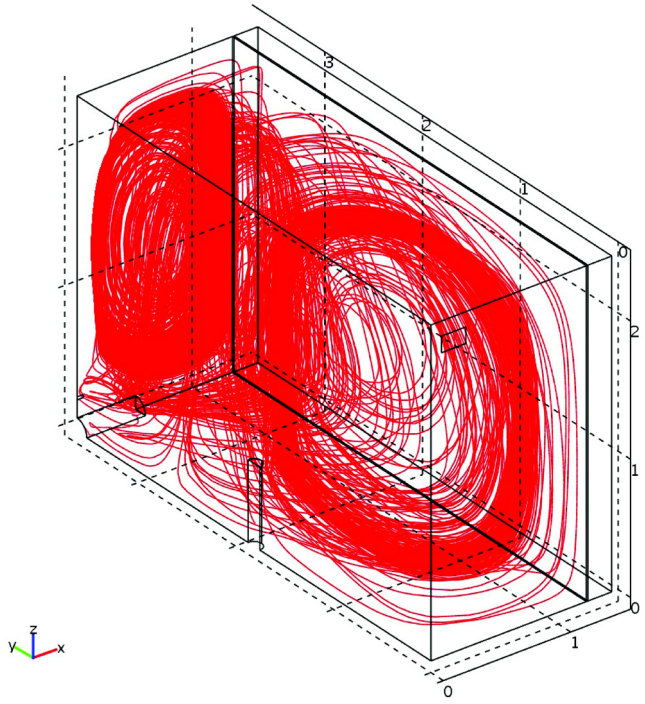

Figure 10 *Streamlines illustrating the velocity field in case 4.*

reason for this change of the distribution profile and the reduction of the temperature and RH was that stronger ventilation changes the air movement pattern inside the test room and carries away more heat and moisture.

Increasing ventilation outlet size had less effect on both air temperature and RH level, which indicates that outlet size is not an important factor to influence the air, heat, and moisture balance in this simulation model. Since a zero pressure boundary condition was assigned to the outlet, the convective flux for heat and mass (moisture) did not change significantly as the dimension of the boundary (outlet) changed.

Different ventilation conditions have different impacts on heat and moisture transfer through the envelope. Table 2 shows the integration of heat and moisture fluxes across the interstitial boundary between subdomains 2 and 3 in all four cases. Since the same outdoor conditions were used in the simulation of all cases, the heat and moisture fluxes in the walls are related to the indoor temperature, RH profile, and velocity along the wall surface.

The velocity profiles near the interior surface of wood paneling for cases 1 and 4 are presented in Figures 11 and 12, respectively. Compared to that of case 1, case 4 had a different pattern but similar magnitude of air velocity. It was also noticed that higher velocities are obtained in case 2 (figures for cases 2 and 3 are not included). That is evidently related to the higher ventilation rate simulated in case 2. The enlarged ventilation outlet (case 3) only changed the velocity profile at the corner close to the vent.

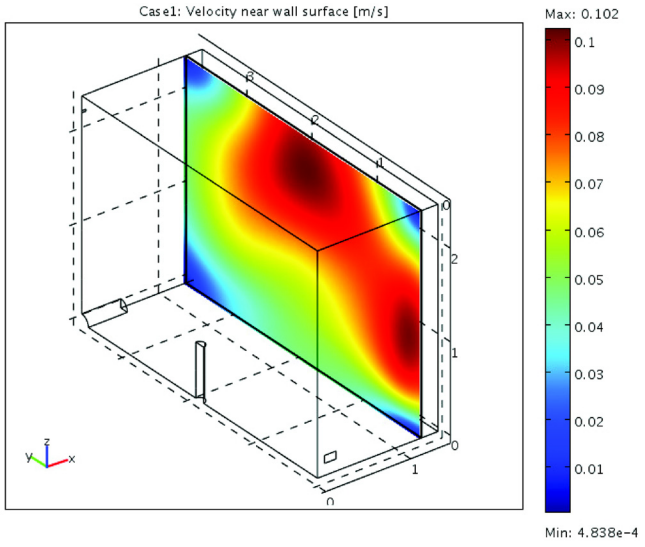

Figure 11 *Velocity distribution on the plane 0.02 m away from the south wall surface in case 1.*

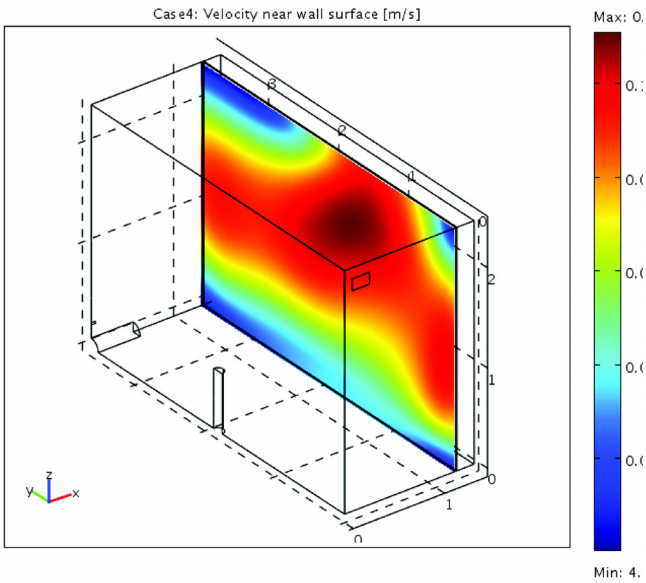

Figure 12 *Velocity profile on the plane 0.02 m away from the south wall in case 4.*

Table 2. Total Heat and Moisture Fluxes Passing through Interstitial Boundary between Subdomains 2 and 3

	Heat Flux, W	Moisture Flux, kg/s
Case 1	45.99	5.323×10^{-8}
Case 2	46.03	4.027×10^{-8}
Case 3	45.92	5.467×10^{-8}
Case 4	50.62	8.652×10^{-8}

Theoretically, the higher velocity close to the wall surface should lead to higher surface coefficients and increase the heat and mass fluxes through the wall systems. In this simulation, increased velocity in case 2 did not result in a bigger moisture flux, and the nearly equal velocity value in case 4 obtained the higher transfer fluxes of heat and moisture. This indicates that, under mixed ventilation, heat and mass transfer inside walls is influenced by surface transfer coefficient much less than by the indoor temperature and humidity level.

CONCLUSION

A CFD model coupled momentum, heat, and moisture transport inside a test room and through multilayered wall systems has been established. The coupling means among the governing equations and between the indoor room domain and the wall system domain in a single simulation environment (COMSOL) has been presented. Using this model, the indoor condition, HAM transport in the wall, ventilation efficiency, and other coupled processes could be directly simulated. This paper presented the initial results of this model.

Based on this model, the indoor environment and heat and moisture transport through its envelope were found to be influenced by ventilation parameters that included the rate, return vent size, and position of inlet and outlet. The position of the ventilation vents had the most significant effect on the indoor environment. The increased ventilation rate carries away more heat and moisture, and thus reduces the temperature and moisture level inside the room. The change of the ventilation outlet area had the least effect on the indoor environment.

Predictions showed that, under the mixed convection condition, the indoor temperature and moisture level (which changes with the ventilation condition) dominate the heat and moisture transport through the wall system. The velocity profile along wall surface had less effect on the heat and mass transfer inside the walls.

The limitation of this model is that mass coupling on the wall surface is based on the direct continuity of mass flux calculation. As a result, the model may not present well the turbulent effects on the mass transfer in this region. The agreement of the RH and temperature distribution inside the test room with the experimental measurement indicates that, under mixed convection conditions, this model can correctly predict the indoor environment with the HAM responses of the wall system taken into account. Further validation of this model will be performed with additional experimental data.

This model will be developed further to study the influence of room level factors on moisture-buffering effects of the wood paneling.

ACKNOWLEDGMENTS

This project is supported by the Natural Science and Engineering Council of Canada (NSERC). Drs. Sergio Vera

and Xiangjin Yang worked on the initial test setup. Caroline Hachem reviewed a previous draft of the manuscript and contributed to some of the figures.

NOMENCLATURE

β = a model constant, —
ε = the dissipation rate of turbulent energy, m^2/s^3
η_T = the turbulent viscosity, $N \cdot s/m^2$
ρ = fluid density, kg/m^3
δ^+ = dimensionless wall offset, —
σ_k = model constant, —
σ_ε = model constant, —
c = moisture concentration, kg/m^3
C_p = the specific heat capacity, J/kg·K
C_μ = model constant, —
$C_{\varepsilon 1}$ = a model constant, —
$C_{\varepsilon 2}$ = a model constant, —)
d_i = thickness of the i th component, m
D = the diffusion coefficient, $kg/m^3 \cdot s$
I = unit tensor, —
k = turbulent kinetic energy. m^2/s^2
K = the thermal conductivity, W/m·K
k_i = thermal conductivity the i th component, W/m·K
k_T = turbulent conductivity, W/m·K
P_0 = reference pressure, Pa
P = static pressure, Pa
q = heat flux, W/m^2
Q = heat source, W/m^3
R = reaction rate for mass species, $kg/m^3 \cdot s$
V = velocity, m/s

REFERENCES

Amissah, P. 2005. *Indoor air quality—Combining air humidity with construction moisture*. Glasgow, UK: University of Strathclyde, Doctoral thesis.

ASHRAE. 2005. *2005 ASHRAE Handbook—Fundamentals*. Atlanta, GA: American Society of Heating, Refrigerating and Air-Conditioning Engineers, Inc.

COMSOL. 2008. *COMSOL 3.5 multiphysics user's guide*. COMSOL AB.

Erriguible, A., P. Bernada, F. Couture, and M. Roques. 2006. Modeling of heat and mass transfer at the boundary between a porous medium and its surroundings. *Journal of Drying Technology* 23(3):455–72.

Fazio, P., S. Vera, J. Rao, X. Yang, and H. Ge. 2007. *Datasets of whole-building HAM indoor conditions for one-room and vertical two-room experimental setups*. Final Report of Canadian Contributions, Annex 41 of the International Energy Agency (IEA).

Janssen, H. and S. Roels. 2009. Qualitative and quantitative assessment of interior moisture buffering by enclosures, *Energy and Buildings* 41(4):382–94.

Neale, A. 2007. *A study in computational fluid dynamics for the determination of convective heat and vapour transfer coefficients*. Montreal, QC: Concordia University, Thesis of MASc.

Paepe, M. 2008. Advances in 3D airflow modelling. Annex 41, Modelling principles and common exercises. In *Whole building heat, air, moisture response*, M. Woloszyn and C. Rode, eds., p 114–115. International Energy Agency.

Pepper, D.W. and X. Wang. 2009. Benchmarking COMSOL 3.5a—CFD problem. COMSOL Conference, Boston, MA.

Steeman, H.J., A. Janssens, J. Carmeliet, and M. Paepe. 2009. Modelling indoor air and hygrothermal wall interaction in building simulation: Comparison between CFD and a well-mixed zonal model. *Building and Environment* 44(3):572–83.

Van Schijndel, J. 2008. Guidelines for heat and moisture modelling in constructions using multiphysics FEM software. *Building Physics Symposium Leuven*, pp. 59–62.

Vera, S., P. Fazio, and J. Rao. 2010. Interzonal air and moisture transport through large horizontal openings in a full-scale two-story test-hut: Part 1—Experimental study. *Building and Environment* 45(5):1192–1201.

Yang, X., S. Vera, J. Rao, H. Ge, and P. Fazio. 2007. Full-scale experimental investigation of moisture buffering effect and indoor moisture distribution. *Proceedings of Thermal Performance of the Exterior Envelopes of Whole Buildings (Building X Conference)*, Clearwater Beach, FL.